Journal of Oceanography, Vol. 62, pp. 171 to 183, 2006

Seasonal and Interannual Variations in the East Sakhalin Current Revealed by TOPEX/POSEIDON Altimeter Data

NAOTO EBUCHI*

Institute of Low Temperature Science, Hokkaido University, Kita-ku, Sapporo 060-0819, Japan

(Received 8 September 2005; in revised form 9 November 2005; accepted 29 November 2005)

Seasonal and interannual variations in the East Sakhalin Current (ESC) are investigated using ten-year records of the sea level anomaly (SLA) observed by the TOPEX/POSEIDON (T/P) altimeter. The T/P SLA clearly documents seasonal and interannual variations in the ESC along the east coast of Sakhalin Island, although sea ice masks the region from January to April. Estimates of surface current velocity anomaly derived from T/P SLA are in good agreement with drifting buoy observations. The ESC is strong in winter, with a typical current velocity of 30–40 cm s^{-1} in December, and almost disappears in summer. Southward flow of the ESC is confined to the shelf and slope region and consists of two velocity cores. These features of the ESC are consistent with short-term observations reported in previous studies. Analysis of the ten-year records of T/P SLA confirms that the structure of the ESC is maintained each winter and the seasonal cycle is repeated every year, although the strength of the ESC shows large interannual variations. Seasonal and interannual variations in the ESC are discussed in relation to wind-driven circulation in the Sea of Okhotsk, using wind stress and wind stress curl fields derived from European Centre for Medium Range Weather Forecasts (ECMWF) reanalysis data and a scatterometer-derived wind product. Seasonal and interannual variations of the anticyclonic eddy in the Kuril Basin are also revealed using T/P SLA.

Keywords:
· East Sakhalin Current,
· Sea of Okhotsk,
· TOPEX/POSEIDON,
· satellite altimetry.

1. Introduction

The East Sakhalin Current (referred to as ESC hereafter) flows southward along the east coast of Sakhalin Island in the Sea of Okhotsk. The ESC is important for the transport of dense shelf water (DSW; Kitani, 1973; Talley, 1991), which forms in the northern shelf region of the Okhotsk Sea. The DSW is considered to be closely related to ventilation of the North Pacific Intermediate Water (NPIW). The ESC also contributes to the transport of sea ice (Watanabe, 1963; Parkinson and Gratz, 1983). Submarine oil fields have recently been developed on the continental shelf of northeast Sakhalin. In case of an oil spill from the oil fields or tankers cruising in this region, the ESC would likely carry the oil to southern parts of the Okhotsk Sea, causing significant environmental damage.

With the exception of schematics of the surface circulation in the Okhotsk Sea presented in old Russian literature (e.g., Leonov, 1960; Moroshkin, 1966), features of the ESC, including its very existence, have been poorly understood in the past because direct observations of the ESC were very limited. Detailed observations in the area, including direct measurements of the surface currents, are hampered by severe winter weather conditions and political issues concerning the Sea of Okhotsk. Most attempts to describe the flow field of the Sea of Okhotsk were based on indirect measurements, such as dynamic topography, water mass analysis, ice motions and ship drifts, or on short-term direct measurements (see the review by Talley and Nagata, 1995).

From 1998 to 2001, intensive direct observation of the current fields in the Okhotsk Sea was undertaken by the Joint Japanese-Russian-U.S. Study of the Sea of Okhotsk. Ohshima *et al*. (2002) deployed 20 drifting buoys in order to observe surface circulation in the Okhotsk Sea and subsequently revealed the existence of the ESC. They demonstrated that the ESC is strongly controlled by bottom topography and is confined within the region shallower than 1000 m. It was also found that the ESC consists of two cores: one near the coast at depths of 50–150 m with typical speeds of 0.3–0.4 m s^{-1}, and another

* E-mail address: ebuchi@lowtem.hokudai.ac.jp

over the shelf slope at 300–900 m depths with typical speeds of 0.2–0.3 m s^{-1}. Mizuta *et al*. (2003) conducted a long-term mooring observation off the east coast of Sakhalin Island from 1998 to 2000 and estimated the annual mean volume transport of the ESC to be 6.7 Sv (1 Sv = 10^6 m^3s^{-1}) with a maximum of 12.3 Sv during February and a minimum of 1.2 Sv during October. Fukamachi *et al*. (2004) investigated transport and modification processes of the DSW using the mooring data combined with hydrographic observations.

To investigate the driving mechanisms of the ESC, Simizu and Ohshima (2002) utilized a barotropic model forced by monthly mean wind stress from the European Centre for Medium-Range Weather Forecasts (ECMWF) reanalysis with realistic bottom topography. They suggested that the nearshore core of the ESC can be interpreted as arrested topography waves (ATW): a coastal current driven by the alongshore wind stress (Csanady, 1978). Ohshima *et al*. (2004) showed that the Sverdrup balance holds roughly in the cyclonic gyre over the northern half-basin of the Okhotsk Sea (50–53°N) and that a major part of the ESC can be regarded as the western boundary current of this gyre. Simizu and Ohshima (2006) simulated both cores of the ESC using the Princeton Ocean Model with realistic bottom topography and wind forcing.

Intensive observations under the Joint Japanese-Russian-U.S. Study of the Sea of Okhotsk revealed various features of the ESC, such as its width, extension, velocity structure, volume transport and seasonal variability. However, these results were generally based on data obtained during a limited period of just a few years. While numerical model experiments provide some additional insight into the nature of the interannual variations, it is necessary to assess the robustness of our current understanding of features of the ESC and their interannual variability.

In the present study, seasonal and interannual variations in the ESC are investigated using ten-year records of sea level anomaly acquired by the TOPEX/POSEIDON (T/P) altimeter. Satellite altimetry provides vital information on temporal variations in the region of the ESC, where *in situ* observations are limited in number and in terms of their spatial and temporal coverage. Data utilized in the present study are introduced briefly in Section 2. Comparison of the altimeter-derived sea level anomaly data with *in situ* drifting buoy observations is described in Section 3, while Section 4 describes seasonal variation in the ESC as observed by T/P. Section 5 discusses interannual variability in the ESC, while seasonal and interannual variations in the anticyclonic eddy in the Kuril Basin are described in Section 6. A brief summary and concluding remarks are provided in Section 7.

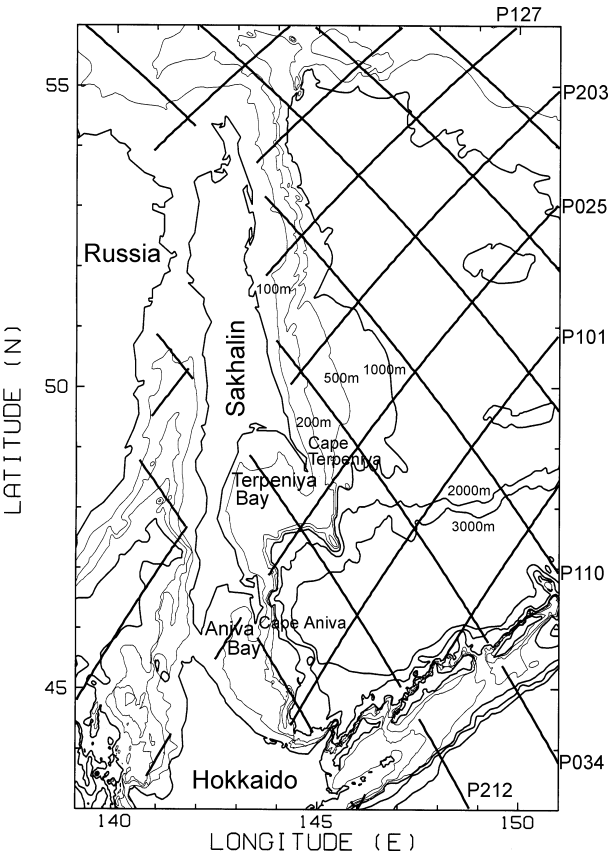

Fig. 1. Bathymetry of the southwest Okhotsk Sea and locations of TOPEX/POSEIDON altimeter ground tracks.

2. Data

2.1 Sea level anomaly

The TOPEX/POSEIDON Sea Level Anomaly (SLA) altimeter product for the entire duration of the T/P mission, from October 1992 to March 2002 (cycles 2-351), was analyzed in the present study. The product was provided by the Collecte Localisation Satellites (CLS) Space Oceanography Division, Toulouse, France (AVISO/ Altimetry, 1998). The SLA product was generated using the conventional repeat-track analysis method from altimeter sea surface heights corrected for instrumental errors, environment perturbations (wet tropospheric, dry tropospheric and ionospheric effects), ocean wave influence (sea state bias), tide influence (ocean tide, earth tide and pole tide) and inverse barometric effect. The CLS Mean Sea Surface was used to correct for cross-track geoid gradient errors. Corrections were also made for long wavelength errors (LWE) due to residual orbit errors, tidal or inverse barometer errors, and high frequency ocean signals. The sea surface height anomalies were calculated

relative to 7-year averages (January 1993 to January 1999) and were resampled every 7 km for a given track and for each cycle. The temporal interval of the repeat cycle is 9.91 days. Locations of the ground tracks analyzed in this study and the bathymetry of the southwest Okhotsk Sea are shown in Fig. 1.

Spatial filtering was not applied to the SLA, as the ESC is confined to a narrow coastal region (Ohshima *et al.*, 2002) and is therefore susceptible to smearing by the filtering process. In the coastal regions of a marginal sea, correction for the ocean tide using a global tide model can generate large errors. To reduce the errors in the SLA resulting from the tide correction, harmonic analysis for aliasing periods of the eight main tidal constituents (Schlax and Chelton, 1994; Ebuchi and Hanawa, 1996) was applied and variations with the aliasing periods were subtracted from the SLA.

2.2 Surface wind data

Due to the scarcity of *in situ* wind observations, two wind data sets were used to estimate wind-driven surface circulation in the Sea of Okhotsk: ECMWF reanalysis data (ERA40) and French Research Institute for Exploitation of the Sea (IFREMER) mean wind fields (MWF). Spatial resolution of the ERA40 is approximately 1.125°, while the temporal interval is 6 hours. Surface wind stress was calculated using the bulk formula with drag coefficient proposed by Smith (1988). Monthly averaged wind stress and wind stress curl fields were calculated from the surface wind stress fields of the 6-hour interval for the period from 1992 to 2002.

The IFREMER MWF (IFREMER, 2002) product was composed from spaceborne scatterometer observations by the Active Microwave Instrument (AMI) aboard the European Remote Sensing Satellite (ERS)-1 and -2 and SeaWinds on QuikSCAT using the kriging technique (Bentamy *et al.*, 1996). The kriging technique is an objective method of interpolating swath observations onto regular grids in time and space. Spatial resolution of the MWF is $1° \times 1°$. The drag coefficient proposed by Smith (1988) was used to calculate wind stress. Monthly mean wind stress and wind stress curl products for the period from 1992 to 2002, which were produced directly from the scatterometer swath observations using the kriging interpolation scheme (IFREMER, 2002), were utilized in the present study.

2.3 Drifting buoy observations

To evaluate the accuracy of sea surface height observed by the T/P altimeter in the continental self and slope region east of Sakhalin, the altimeter-derived SLA was compared with *in situ* observations by surface drifters (Ohshima *et al.*, 2002). The surface current velocity observed by the drifting buoys was also used to estimate the mean current velocity by combination with the altimeter data and to compose the absolute current velocity. Ohshima *et al.* (2002) deployed twenty ARGOSS buoys with a holey sock drogue at a depth of 15 m in the Sea of Okhotsk to observe the ESC during the period from August to September 1999 (see their figure 2 for buoy trajectories). Most of the buoys drifted along the ESC and provided Lagrangian observations of the surface currents until February 2000. Tidal current was approximately removed using a 25-hour running mean. Daily mean locations and velocities of the drifting buoys were utilized in the present study. Details of the drifting buoy observation and data processing are described by Ohshima *et al.* (2002).

3. Comparison of T/P SLA with *In Situ* Drifting Buoy Measurements

To confirm that the altimeter-derived SLA is applicable to the ESC region, the T/P SLA is compared with the daily mean surface velocity as observed by the drifting buoys. Cross-track velocity anomaly is calculated from the SLA by assuming geostrophy as

$$u_a' = \frac{g}{f}\frac{\partial \eta'}{\partial s} \tag{1}$$

where u_a' is the cross-track component of the surface velocity anomaly, η' the SLA, f the Colioris parameter, g the acceleration of gravity, and s the distance along the altimeter ground track.

The daily drifting buoy observations were collocated with the altimeter data by selecting only the buoy data obtained within 0.5° latitude and 0.1° longitude of the altimeter observation point at a temporal separation of less than 5 days. The temporal mean cross-track velocity $\bar{u}$ is estimated by combining the drifting buoy data with the altimeter observations as described by Uchida and Imawaki (2003) and Imawaki *et al.* (2003):

$$u_d(x,t) = \bar{u}(x) + u_a'(x,t) \tag{2}$$

where $u_d(x, t)$ is the cross-track component of the surface velocity measured by the drifting buoys at point x and time t, $\bar{u}(x)$ is the mean cross-track velocity component at that same point, and $u_a'(x, t)$ is the anomaly of the cross-track velocity component derived from the SLA at that same point and time. The anomaly of the cross-track velocity component derived from the drifting buoy measurement, $u_d'(x, t)$, can be derived by subtracting the mean velocity, as follows

$$u_d'(x,t) = u_d(x,t) - \bar{u}(x). \tag{3}$$

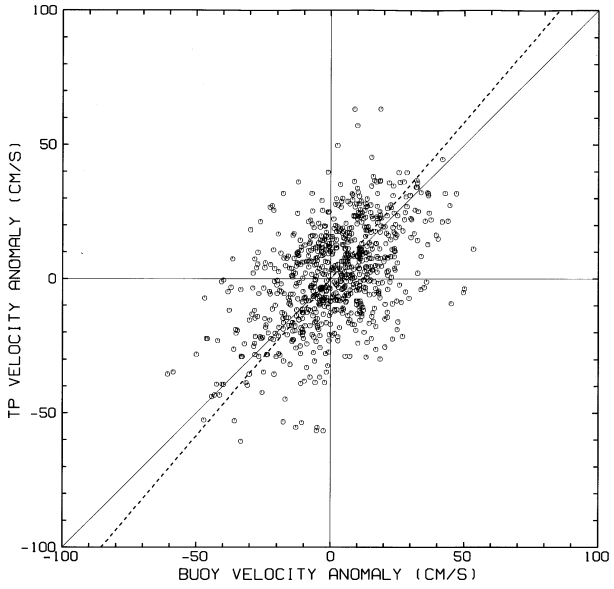

Fig. 2. Comparison of the cross-track velocity anomalies estimated from drifting buoy measurements and altimeter-derived SLA. The dashed line represents the regression line calculated by principle component analysis.

For multiple collocated data at a single point, an ensemble average of $\bar{u}(x)$ is calculated to derive the velocity anomaly. In the present study, only those points that contained more than three collocated data are selected for the comparison and composition of the absolute velocity. The magnitude of the mean cross-track velocity in the ESC region is estimated to be 15–20 cm s^{-1}. Because of sea ice coverage in winter, the SLA and cross-track velocity anomaly, η' and u_a', were calculated relative to averages over a period from May to December in the years from 1992 to 2001. Selection of the average period may change the mean velocity, $\bar{u}(x)$, but does not affect the comparison of the velocity anomalies and absolute cross-track velocity composed by $\bar{u}(x) + u_a'(x, t)$.

Figure 2 shows a comparison of cross-track velocity component anomalies estimated from drifting buoy measurement (u_d') and altimeter-derived SLA (u_a'). Most of the data are located in the shelf and slope region east of Sakhalin Island. The number of data points is 772, the root-mean-squared (rms) difference is 18.2 cm s^{-1}, the correlation coefficient is 0.503, and the slope of regression line calculated by principal component analysis is 1.17. Although the correlation coefficient is relatively low, the rms difference is similar to or slightly larger than those obtained by comparisons of surface velocities derived by the T/P altimeter with *in situ* ADCP observations (e.g., Ebuchi and Hanawa, 1995; Uchida and Imawaki, 2003; Imawaki *et al.*, 2003). However, the rms difference may not be small enough to resolve seasonal variation in the ESC, which is approximately 30–40 cm s^{-1} (Ohshima *et al.*, 2002; Mizuta *et al.*, 2003; and see also Sections 4 and 5). Note that the rms difference includes not only errors in the altimeter observation in the coastal region but also errors in the drifting buoy measurements and the estimation of the mean velocity together with influences of temporal and spatial separations. In the following sections, therefore, monthly averages (i.e., three-point ensemble averages in time) of the SLA and cross-track velocity component are utilized in order to reduce the random errors.

4. Seasonal Variation of the East Sakhalin Current

Monthly averaged SLAs were calculated for each altimeter ground track according to the results described in Section 3. Averages were then calculated over the entire period of the T/P mission, from October 1992 to March 2002, for each month in order to illustrate seasonal variation in the ESC as a long-term average. Only those data points were used for which the mean SLA was calculated from monthly data over more than five years. Figure 3 shows the ten-year average SLA with standard deviation. SLA profiles are only shown for May to December, as in most years this region is covered by sea ice from January until April.

SLA profiles along Passes 127, 203, 110, and 034 show clear seasonal variation associated with the ESC. From October to December, the SLA increases towards the east coast of Sakhalin, indicating the existence of a southward cross-tack velocity anomaly. The difference in SLA and the width of the ESC are estimated to be roughly 10–15 cm and 70 km (approximately 1° in longitude), respectively. From May to September, the SLA profiles show the opposite slope, toward the coast, as the annual mean SLA must equal zero. However, we cannot determine from the SLA alone whether a northward current exists or the southward ESC simply weakens during these months. The two cores of the ESC, which were first discovered by Ohshima *et al.* (2002), are not clearly imaged in these profiles.

During November and December, there is a peak of SLA along Pass 025, off Cape Terpeniya (at about 145°E in Fig. 3(a)), indicating that the ESC turns clockwise and flows into Terpeniya Bay. The ESC also appears in the SLA profiles along Pass 212 as a pronounced slope at 144–145°E. At 146°E, along Pass 212, a positive peak in SLA indicates an anticyclonic eddy in the southwest Kuril Basin from September to November. The SLA variations associated with this eddy are described in Section 6.

Figure 4 shows the horizontal distribution of cross-track velocity anomalies from October to December, which was calculated via Eq. (1) from the SLA profiles shown in Fig. 3. The velocity anomaly profiles were smoothed by applying a three-point running average. In

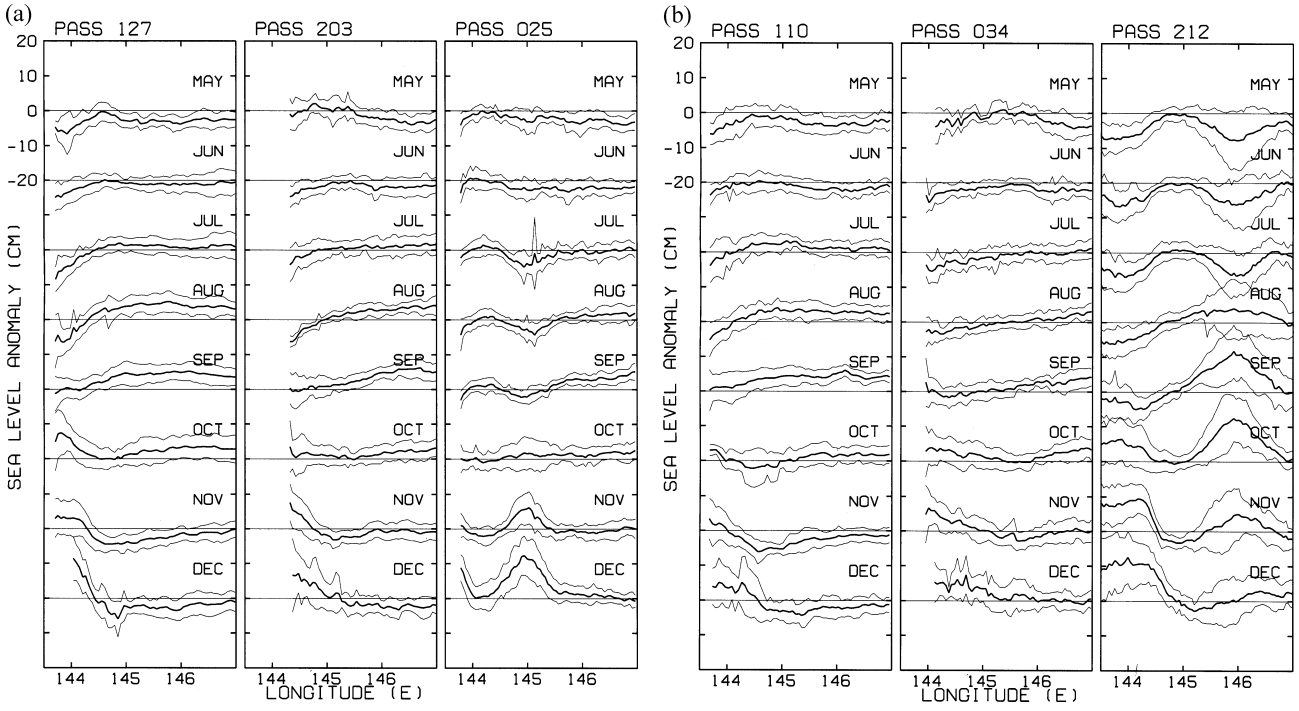

Fig. 3. Seasonal variation in the SLA observed along (a) ascending passes (Pass 127, 203, and 025), and (b) descending passes (Pass 110, 034, and 212). Monthly SLA profiles averaged over ten years from 1992 to 2001 (thick lines) and their standard deviations (thin lines).

December (Fig. 4(c)), some of the data for the north and east coast of Sakhalin Island are missing because of sea ice coverage. In October (Fig. 4(a)), the largest velocity anomaly is found at the anticyclonic eddy in the Kuril Basin, as described above. The magnitude of the velocity anomaly reaches up to 20–30 cm s^{-1}. Along the northern part of Sakhalin Island, eastward and southward velocity anomalies associated with the ESC are discernible, though their magnitude is low (10–15 cm s^{-1}).

The anticyclonic eddy in the Kuril Basin weakens in November (Fig. 4(b)) and the ESC becomes stronger. To the north of Sakhalin Island (around 55°N, 141–143°E), the cross-track velocity anomalies indicate an eastward flow of the ESC, while along the east coast of Sakhalin (49–54°N, 144–146°E), the ESC flows southward with cross-track velocity anomalies up to 30 cm s^{-1}. Southeast of Cape Terpeniya, the velocity anomaly suggests that the ESC turns westward and flows into Terpeniya Bay. Ohshima *et al.* (2002) reported that the ESC splits into two parts, with one part turning eastward and the other continuing to flow south as far as the southern tip of Sakhalin. In Fig. 4(b) the eastward branch of the ESC does not appear clearly to the east of 146°E. It can be speculated that the eastward branch of the ESC has low variability and does not appear in the SLA and velocity anomaly profiles. A climatic map of the geopotential anomaly in the Sea of Okhotsk (figure 2 of Ohshima *et al.*, 2004) suggests the existence of the mean eastward flow in this region. Further studies combining *in situ* and altimetry observations are needed to clarify this discrepancy. To the south of Terpeniya Bay, a southward flow is discernible along the coast and continues south past Cape Aniva toward the northern coast of Hokkaido. Similar patterns are observed in December (Fig. 4(c)) and the magnitude of the cross-track velocity anomaly is amplified to 30–35 cm s^{-1}.

Seasonal variation in the absolute velocity associated with the ESC can be composed by combining the mean cross-track velocity with the cross-track velocity anomalies shown in Fig. 4. An example for Pass 127 is shown in Fig. 5. As described in Section 3, the mean cross-track and absolute velocities are estimated at only those points that contained more than three buoy-altimeter collocated data. The absolute cross-track velocity (arrows) for May is plotted at a location of the ground track east of Sakhalin Island. The profiles from June to December are plotted by shifting to the right to avoid overlap. In the profile for December, the three points located closest to the coast are missing because of sea ice coverage. The lower subpanel represents the absolute cross-track velocity averaged over this section of Pass 127.

The absolute cross-track velocities clearly show sea-

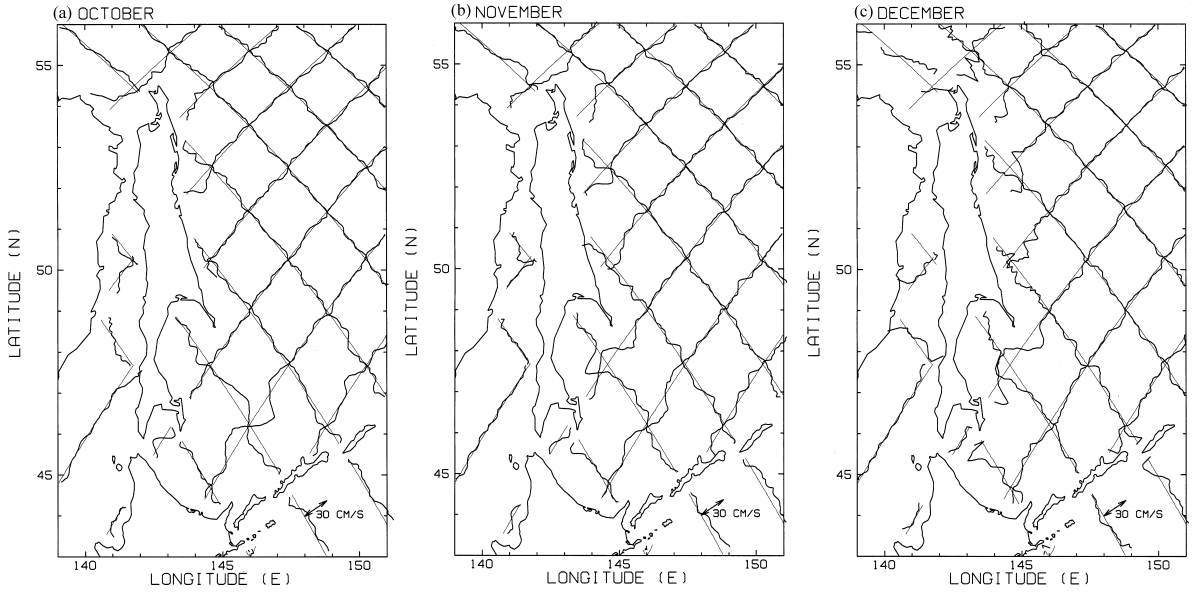

Fig. 4. Cross-track velocity anomalies calculated from the ten-year mean SLA profiles. (a) October, (b) November, and (c) December.

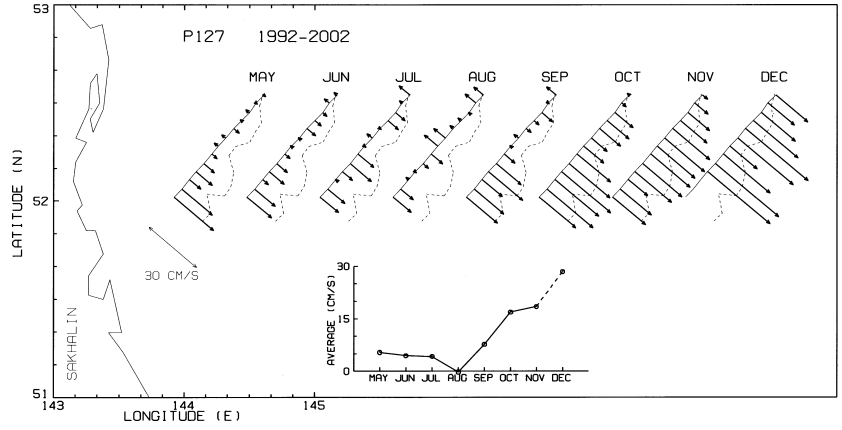

Fig. 5. Seasonal variation in the absolute cross-track velocity along Pass 127. The absolute cross-track velocity (arrows) for May is plotted at a location east of Sakhalin Island where the mean velocity (dashed line) was estimated. The profiles from June to December are plotted by shifting to the right to avoid overlap. The lower subpanel represents the cross-track velocity averaged over this section of the ground track.

sonal variation in the ESC. During summer the southward velocity is very weak, increasing through autumn and winter. The maximum cross-track component of the absolute velocity reaches 40 cm s^{-1}. No strong northward current is discernible even in summer, although the SLA profiles in Fig. 3 indicate northward velocity anomalies. Most of these features of the ESC are consistent with the discovery of Ohshima *et al.* (2002) derived from drifting buoy observations and of Mizuta *et al.* (2003) using moored current measurements.

Absolute surface current vectors are composed by combining the absolute cross-track velocities estimated along Passes 127 (Fig. 5) and 110 in the region east of Sakhalin Island between 52°N and 53°N. A pair of the cross-tack velocities derived at the same longitude along the two altimeter passes are combined to calculate the velocity vector assuming that the ESC flows along the bottom topography and the coast line and isobaths are approximately in the meridional direction in this region (Ohshima *et al.*, 2002). Figure 6 shows seasonal variations of the zonal profile of the absolute surface velocity vectors. Water depth contained in the ETOPO5 global

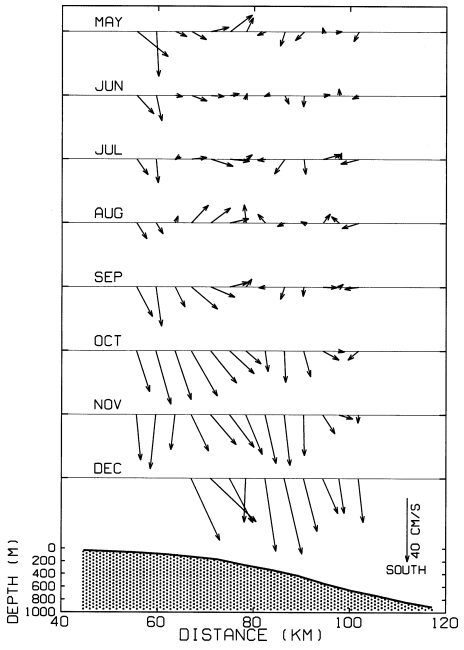

Fig. 6. Seasonal variation in the absolute surface current vectors in the region east of Sakhalin Island between 52°N and 53°N composed by combining the absolute cross-track velocities estimated along Passes 127 and 110. The horizontal axis is zonal distance from the coast line. Thick line with shading represents the mean bottom topography in the region.

earth topography data is averaged in the region between 52°N and 53°N and is also shown in the figure.

The two velocity cores of the ESC are clearly visible in the profiles of surface current vectors from September to December, as reported by Ohshima *et al*. (2002), although most of the nearshore core is masked by sea ice in December. The maximum current speeds reach 30 cm s^{-1} in October, 35 cm s^{-1} in November, and 50 cm s^{-1} in December, respectively. In September and October, the nearshore core is stronger than the offshore core, while both cores have the same magnitude in November.

5. Interannual Variations of the East Sakhalin Current

To explore interannual variations in the ESC, the SLA profiles observed along the ground tracks east of Sakhalin in November for the years from 1992 to 2001 are plotted in Fig. 7. Those features of the SLA associated with the ESC as described in the previous section are observed in most years, although the magnitude of the SLA varies markedly from year to year. Slopes of the SLA towards the coast of Sakhalin (Passes 127, 203, 110, and 034), which represent the intensity of the ESC, appear to be enhanced in 1995 relative to the other years.

Figure 8 shows interannual variation in the absolute surface current vectors in the region between 52°N and 53°N during November, calculated from data along Passes

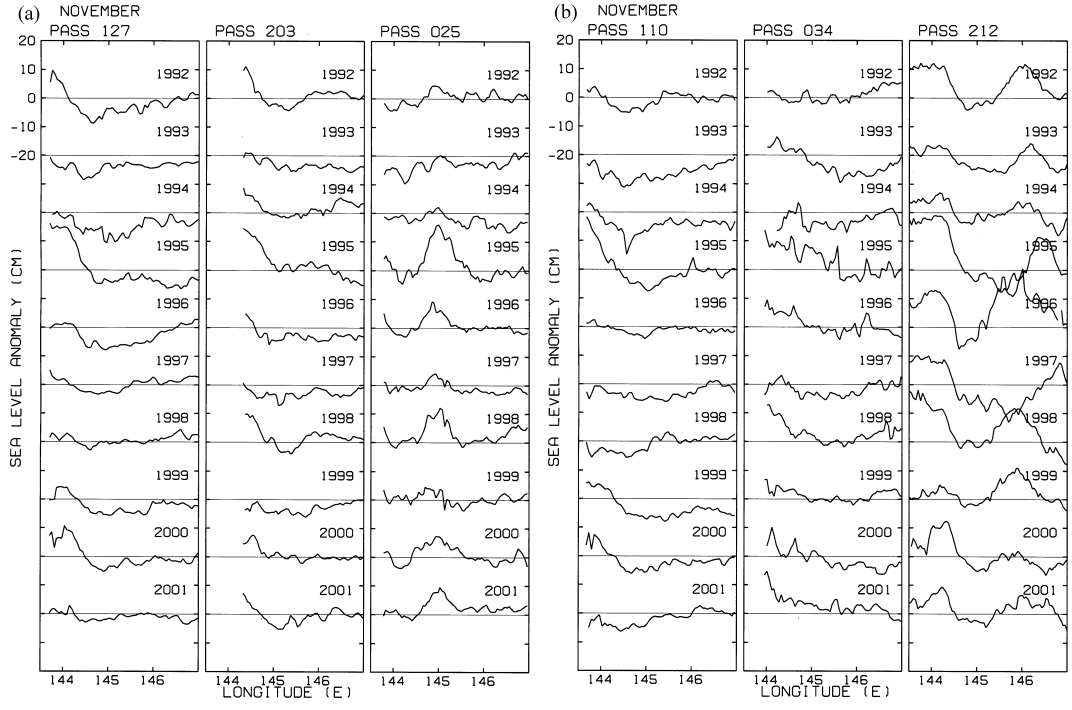

Fig. 7. Profiles of the SLA observed along the ground tracks east of Sakhalin in November from 1992 to 2001.

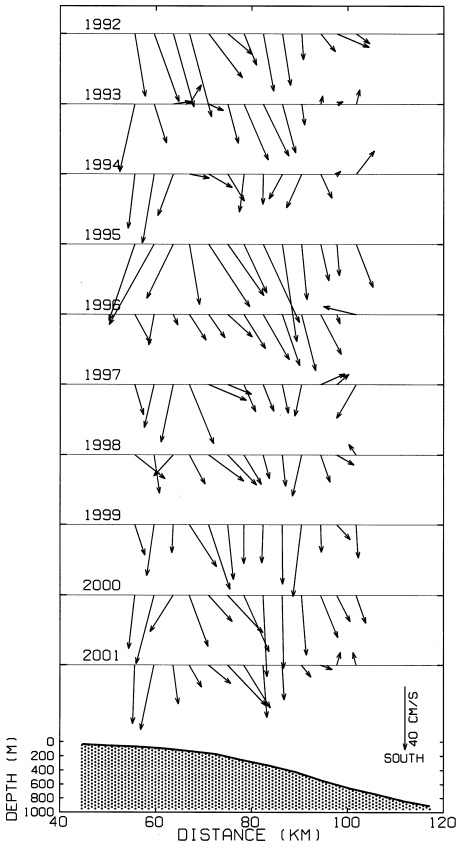

Fig. 8. Interannual variation in the absolute surface current vectors in November of years from 1992 to 2001 in the region east of Sakhalin Island between 52°N and 53°N, composed by combining the absolute cross-track velocities estimated along Passes 127 and 110. The horizontal axis is zonal distance from the coast line. Thick line with shading represents the mean bottom topography in the region.

127 and 110, as for Fig. 6. The intensity of the ESC shows large interannual variations. The ESC is stronger in 1995 and 2001 and maximum velocity exceeds 50 cm s^{-1} in these years. Every year the ESC has two velocity cores, as reported by Ohshima *et al.* (2002) and Mizuta *et al.* (2003), and the both cores appear at almost the same locations.

As discussed by Simizu and Ohshima (2002), Ohshima *et al.* (2004), and Simizu and Ohshima (2006), the driving mechanism of the ESC is considered to be closely related to wind stress over the Sea of Okhotsk. Figure 9 shows the scatterometer-derived wind stress vectors and their curl for November, averaged over the period from 1992 to 2001. The winter wind stress curl is positive over most of the Okhotsk Sea, except for the northeast coast of Sakhalin. This positive wind stress curl generates the cyclonic gyre over the northern part of the Sea of Okhotsk. A major part of the ESC is considered to be the western boundary current of this cyclonic gyre (Ohshima *et al.*, 2004).

The Sverdrup volume transport, M_S, is calculated as

$$M_S = -\frac{1}{\beta\rho}\int_{x_e}^{x} curl\,\vec{\tau}\,dx \qquad (4)$$

where a right-handed Cartesian coordinate system is adopted with x and y axes in the eastward and northward directions, respectively. β is the y derivative of the Coriolis parameter, ρ the density of water, and $\vec{\tau}$ the wind stress vector. The path of integration is taken along latitudinal lines from the eastern boundary x_e to x.

Simizu and Ohshima (2002, 2006) reported that the nearshore core of the ESC can be interpreted as arrested topography waves (ATW), which is a coastal current driven by the alongshore wind stress (Csanady, 1978). According to Csanady (1978), the alongshore component of the vertical integrated velocity of the ATW, V, is given as

$$\int_0^{\infty} V dx' = \int_{y'}^{\infty} \frac{\tau_{y'}}{\rho f}\,dy' \qquad (5)$$

where a right-handed coordinate system is used with the x' axis in the offshore direction and the y' axis along the coastline at $x' = 0$. $\tau_{y'}$ is the alongshore component of the wind stress. Equation (5) implies that the alongshore transport at y' is the sum of all backward Ekman transport to or from the coast (Simizu and Ohshima, 2002, 2006). The total alongshore volume transport by the ATW, M_{ATW}, is estimated by

$$M_{ATW} = -\int_{y_0'}^{y'} \frac{\tau_{y'}}{\rho f}\,dy' \qquad (6)$$

where y_0' is the starting point of the integral, which is determined by considering the shape of the coastline.

In the present study the volume transports expressed by Eqs. (4) and (6) are calculated from the monthly mean wind stress fields from the ERA40 reanalysis and IFREMER MWF scatterometer wind product. According to Simizu and Ohshima (2002, 2006) and Ohshima *et al.* (2004), the starting point of the integration of the Sverdrup transport, x_e, in Eq. (4) was set to the 500-m depth contour, as the wind stress curl in shallow areas is considered to contribute only slightly to wind-driven circulation and volume transport. The starting point of the integration for the ATW volume transport, y_0', in Eq. (6) was selected to be west of Shelikhov Bay (59°N, 155°E), according to Simizu and Ohshima (2002, 2006). The integration was performed along the northern and western

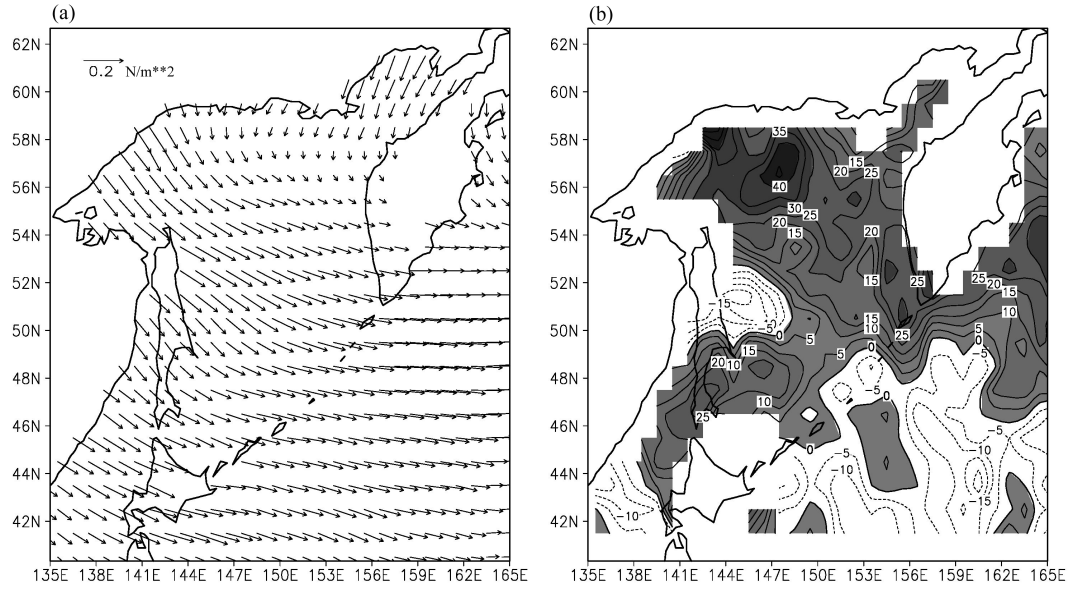

Fig. 9. Scatterometer-derived (a) wind stress vectors and (b) wind stress curl for November averaged over the period from 1992 to 2002. The unit of the contours in the panel (b) is 10^{-8} N m^{-3}, and the area of positive wind stress curl is shaded.

coastline.

Figure 10 shows interannual variations in SLA difference along Passes 110 and 127, and the Sverdrup and ATW volume transports calculated from the wind stress and wind stress curl. The difference between the SLA averaged over the three points closest to the coastline and that averaged from 145°E to 146°E was calculated for November from 1992 to 2001 in order to represent surface transport across the altimeter ground tracks. The SLA differences along Passes 110 and 127 show similar interannual variations. The Sverdrup and ATW transports were also calculated for November from 1992 to 2001 at 53°N. Although the Sverdrup volume transport is much larger than the ATW transport, the surface velocity associated with the ATW is slightly higher than that of the western boundary current (Simizu and Ohshima, 2006). Both of the volume transports estimated from the wind stress field are similar to the SLA differences, although some discrepancies exist. The maximum transports and SLA differences were recorded in 1995. The contribution of the surface current close to the coast, which cannot be observed by the altimeter, may have obscured the relationship. The Sverdrup and ATW volume transports estimated from the wind stress fields of the ECMWF ERA40 and IFREMER MWF show similar variations.

Figure 11 shows seasonal variations in the Sverdrup and ATW volume transports and SLA differences along Passes 110 and 127. Seasonal variation in the ESC is represented by the SLA differences, as discussed in the previous section. The Sverdrup and ATW transports show similar seasonal variations. The results shown in Figs. 10

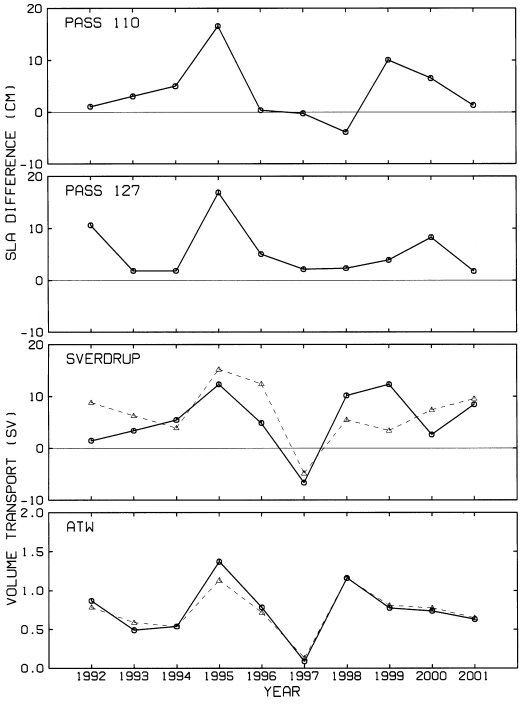

Fig. 10. Interannual variations in the SLA difference along Passes 110 and 127, and Sverdrup and ATW volume transports calculated from the wind stress and wind stress curl in November. Thick circles with solid lines and thin triangles with dashed lines represent the volume transports estimated from the ERA40 and IFREMER MWF, respectively.

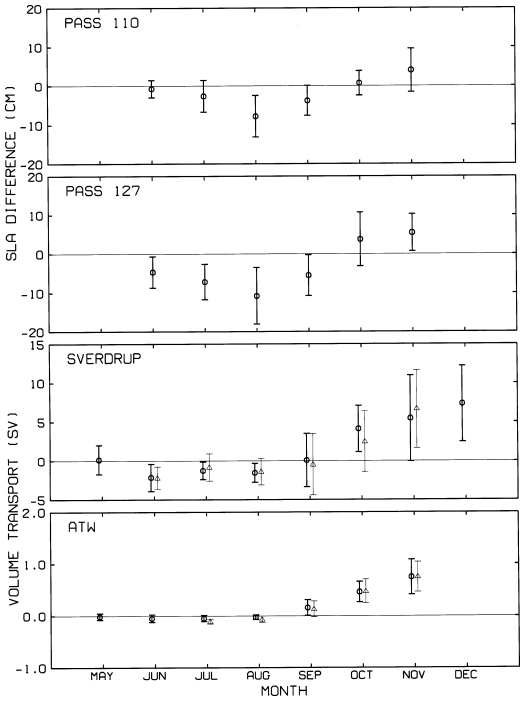

Fig. 11. Seasonal variations in the SLA difference along Passes 110 and 127, and Sverdrup and ATW volume transports calculated from the wind stress and wind stress curl. Monthly averages over the period from 1992 to 2001 are shown with standard deviations. Thick circles and thin triangles represent the volume transports estimated from the ERA40 and IFREMER MWF, respectively.

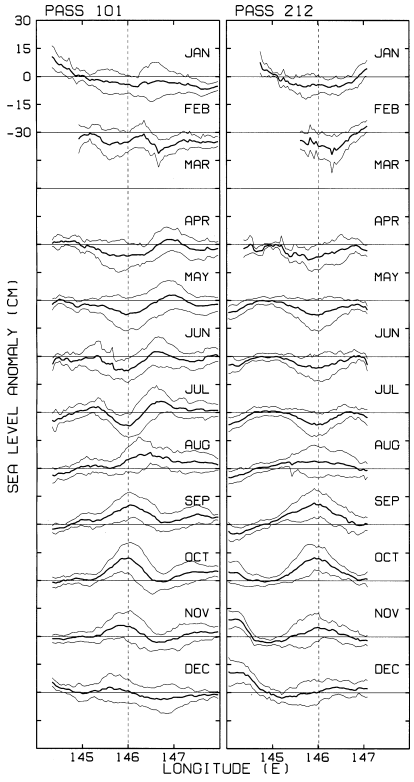

Fig. 12. Seasonal variation in the SLA observed along Passes 101 and 212. Monthly SLA profiles averaged over ten years from 1992 to 2001 (thick lines) and their standard deviations (thin lines). Dashed vertical lines denote the location of the crossover point of the two passes.

and 11 indicate that the seasonal and interannual variations in the ESC are in concert with variations in the wind fields over the Sea of Okhotsk.

The Sverdrup dynamics is controlled by the basin-wide wind forcing, whereas the ATW dynamics depends only on the local wind forcing along the coast. In Figs. 10 and 11, however, the Sverdrup and ATW volume transports show similar seasonal and interannual variations, suggesting that the basin-wide wind and the local alongshore wind are correlated on the seasonal to interannual timescales. It is difficult to separate contributions of the Sverdrup and ATW components to the variations of the ESC from the analysis of altimetry data alone, as conducted in this study. Numerical experiments by Simizu and Ohshima (2006) indicated that the offshore and nearshore cores of the ESC are interpreted in terms of the Sverdrup and ATW dynamics, respectively.

6. An Anticyclonic Eddy in the Kuril Basin

In Figs. 3 and 4, an anticyclonic eddy was found in the southwest part of the Kuril Basin from September to November. This eddy has also been observed from hydrographic data (Wakatsuchi and Martin, 1990, 1991) and satellite infrared imagery (Wakatsuchi and Martin, 1990; Bulatov *et al.*, 1999). Ohshima *et al.* (2002) directly measured the surface velocity field associated with the eddy using drifting buoys.

Figure 12 shows seasonal variation in the SLA observed along two altimeter ground tracks (Passes 101 and 212), which run across the southern Kuril Basin. As in Fig. 3, monthly mean profiles of the SLA were averaged over the period from 1992 to 2001. A peak in the SLA, associated with the anticyclonic eddy, is discernible near the crossover point of these ground tracks (46.2°N, 146°E) from September to November. The peak reaches 15 cm during October. As shown in Fig. 4(a), the maximum magnitude of the velocity anomaly is 20–30 cms^{-1} during October. The diameter of the anticyclonic eddy is estimated to 130 km on an average. The eddy does not appear to move either away from or to any direction.

Interannual variation in the SLA profiles observed in October along two ground tracks is shown in Fig. 13. The anticyclonic eddy is observed most years at the almost same location, although the magnitude of the SLA

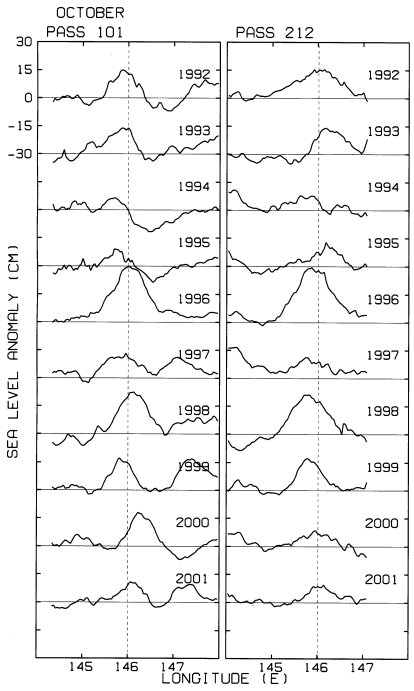

Fig. 13. Interannual variation in the SLA profiles observed in October along Passes 101 and 212. Dashed vertical lines denote the location of the crossover point of the two passes.

peak varies by up to 30 cm. The magnitude of the SLA peak shown in Fig. 13 does not represent the intensity of the anticyclonic eddy, however, as the T/P ground tracks do not always pass through the center of the eddy. Variations in the intensity and location of the eddy influence the magnitude of the SLA peak.

Processes of the generation, maintenance, and decay of the anticyclonic eddy were discussed by Wakatsuchi and Martin (1991). Based on hydrographic observations for a period of three years, they concluded that the formation of the anticyclonic eddy during summer is associated with a deepening of the isopycnals caused by surface flow of the Soya Warm Current over the basin, and the deep advection of cold, less saline water originating from the Sakhalin shelf. During winter, the eddy decays due to surface cooling and convective mixing. The seasonal development of the eddy revealed in Fig. 12 is consistent with their conclusion. Interannual variations exhibited in Fig. 13 reveal that the seasonal cycle of the formation and decay of the eddy is repeated almost every year at the same location. This probably occurs because both of the source waters of the anticyclonic eddy—Soya Warm Current Water and cold, less saline water originating from the Sakhalin shelf (Wakatsuchi and Martin, 1991)—are confined to certain geographical locations due to the bottom topography and have robust seasonal cycles. Uchimoto *et al.* (2006) pointed out that the location and diameter of the anticyclonic eddy depend on the intensity of the Soya Warm Current as a result of numerical experiments.

Bulatov *et al.* (1999) and Ohshima *et al.* (2002) documented a train of anticyclonic eddies in the vicinity of the Kuril Islands. Nakamura and Awaji (2004) simulated the generation of these eddies using a three-dimensional, non-hydrostatic model. Ohshima *et al.* (2005) discussed the generation mechanism of these eddies in relation to strong tidal mixing in and around the Kuril Straits. The eddies were occasionally captured by the T/P SLA, but, it is difficult to trace the eddies using SLA because they move very quickly and are relatively small compared to the spacing of T/P ground track (Bulatov *et al.*, 1999).

7. Summary and Concluding Remarks

The present study has investigated seasonal and interannual variations in the ESC and anticyclonic eddy in the Kuril Basin using ten-year records of SLA observed by the T/P altimeter. The results demonstrate that the altimeter data can be utilized in the coastal region of the marginal sea, although sea ice masks the region from January to April each year. The surface current velocity anomalies are in good agreement with drifting buoy observations.

The T/P-derived SLA clearly captured seasonal and interannual variations in the ESC along the east coast of Sakhalin Island. The ESC is strong in winter, with typical current velocities of 30–40 cm s^{-1} during December, and almost disappears in summer. The ESC is confined to the shelf and slope region, and consists of two velocity cores. These features of the ESC are consistent with the short-term observations reported in previous studies (Ohshima *et al.*, 2002; Mizuta *et al.*, 2003). The robustness of the seasonal evolution and structure of the ESC is confirmed by the ten-year records of the T/P SLA.

The T/P SLA also provides information on interannual variations in the ESC. The strength of the ESC varies markedly from year to year. The interannual variations were discussed in relation to wind-driven circulation in the Sea of Okhotsk. In accordance with previous studies (Simizu and Ohshima, 2002, 2006; Ohshima *et al.*, 2004), Sverdrup and ATW volume transports were estimated using wind stress and wind stress curl from the ECMWF ERA40 reanalysis data and IFREMER scatterometer MWF product. Interannual variations in the volume transports estimated from the wind stress fields are similar to those of the SLA differences along the altimeter ground tracks east of Sakhalin Island, although some discrepancies exist. Data over longer time periods are required to clarify the relationship between the interannual variations in the ESC and those of the wind fields over the Sea of Okhotsk, and to understand the driv-

ing mechanisms of the ESC.

Seasonal and interannual variations in the anticyclonic eddy in the Kuril Basin were also revealed using the T/P SLA. The anticyclonic eddy is located in the southwest Kuril Basin (around 46°N, 146°E) from September to November. The maximum SLA and velocity anomaly in October associated with the eddy are up to 15 cm and 20–30 cms^{-1}, respectively. The eddy has an average diameter of approximately 130 km, and does not appear to move either away from or to any direction. These features are consistent with short-term observations reported in previous studies (Wakatsuchi and Martin, 1990, 1991; Bulatov *et al*., 1999; Ohshima *et al*., 2002). Interannual variation in the SLA profiles reveals that the anticyclonic eddy forms most years in the same location.

The results of the present study demonstrate that altimeter-derived SLA data are useful for investigating surface circulation in the Sea of Okhotsk, although the sea is covered by sea ice for more than four months of the year. A follow-on mission to the T/P, Jason-1, was launched in 2001, and took over the observation of the sea surface heights. Further altimetry missions are also planned. Continuation of sea surface height observation from T/P to Jason-1 and further altimeter missions will provide valuable information concerning interannual variations in the ESC and surface circulation in the Sea of Okhotsk.

Acknowledgements

The author would like to thank Kay I. Ohshima, Yasushi Fukamachi, and Masaaki Wakatsuchi of the Institute of Low Temperature Science, Hokkaido University, and Genta Mizuta of the Graduate School of Environmental Science, Hokkaido University, for providing the *in situ* observation data and for their constructive discussions. The SLA altimeter product utilized in the present study was obtained from the CLS Space Oceanography Division, Toulouse, France. The ERA40 and MWF products were provided by ECMWF and IFREMER, respectively. The present study was supported by a Grant-in-Aid for Scientific Research (B) (No. 15340152) from the Ministry of Education, Culture, Sports, Science and Technology of Japan.

References

AVISO/Altimetry (1998): AVISO User Handbook: Sea Level Anomalies (edition 3.1). AVI-NT-011-312-CN, CLS Space Oceanography Division, Toulouse, France, 24 pp.

Bentamy A., Y. Quilfen, F. Gohin, N. Grima, M. Lenaour and J. Servain (1996): Determination and validation of average wind fields from ERS-1 scatterometer measurements. *Global Atmos. Ocean Sys.*, **4**, 1–29.

Bulatov, N. V., L. A. Kurennaya, L. S. Muktepavel, M. G. Aleksanina and E. E. Gerbek (1999): Eddy water structure in the southern Okhotsk Sea and its seasonal variability (results of satellite monitoring). *Oceanology*, **39**, 29–37.

Csanady, G. T. (1978): The arrested topography wave. *J. Phys. Oceanogr.*, **8**, 47–62.

Ebuchi, N. and K. Hanawa (1995): Comparison of surface current variations observed by TOPEX altimeter with TOLEX-ADCP data. *J. Oceanogr.*, **51**, 351–362.

Ebuchi, N. and K. Hanawa (1996): Comparison of sea surface heights observed by TOPEX altimeter with sea level data at Chichijima. *J. Oceanogr.*, **52**, 259–273.

Fukamachi, Y., G. Mizuta, K. I. Ohshima, L. D. Talley, S. C. Riser and M. Wakatsuchi (2004): Transport and modification processes of dense shelf water revealed by long-term moorings off Sakhalin in the Sea of Okhotsk. *J. Geophys. Res.*, **109**, C09S10, doi:10/1029/2003JC001906.

IFREMER (2002): Mean Wind Field User Manual (version 1.0). C2-MUT-W-05-IF, CERSAT-IFREMER, Plouzane, France, 52 pp.

Imawaki, S., H. Uchida, K. Ichikawa and D. Ambe (2003): Estimating the high-resolution mean sea-surface velocity field by combined use of altimeter and drifter data for geoid model improvement. *Space Sci. Rev.*, **108**, 195–204.

Kitani, K. (1973): An oceanographic study of the Okhotsk Sea: Particularly in regard to cold waters. *Bull. Far Sea Fish. Res. Lab.*, **9**, 45–77.

Leonov, A. K. (1960): *The Sea of Okhotsk*. Natl. Tech. Inf. Serv., Springfield, VA, U.S.A.

Mizuta, G., Y. Fukamachi, K. I. Ohshima and M. Wakatsuchi (2003): Structure and seasonal variability of the East Sakhalin Current. *J. Phys. Oceanogr.*, **33**, 2430–2445.

Moroshkin, K. V. (1966): Water masses of the Sea of Okhotsk. *Joint Pub. Res. Serv. 43942*, U.S. Dept. of Comm., Washington, D.C., 98 pp.

Nakamura, T. and T. Awaji (2004): Tidally induced diapycnal mixing in the Kuril Straits and its role in water transformation and transport: A three-dimensional nonhydrostatic model experiment. *J. Geophys. Res.*, **109**, C09S07, doi:10.1029/2003JC001850.

Ohshima, K. I., M. Wakatsuchi, Y. Fukamachi and G. Mizuta (2002): Near-surface circulation and tidal currents of the Okhotsk Sea observed with satellite-tracked drifters. *J. Geophys. Res.*, **107**, 3195, doi:10.1029/2001JC001005.

Ohshima, K. I., D. Simizu, M. Itoh, G. Mizuta, Y. Fukamachi, S. C. Riser and M. Wakatsuchi (2004): Sverdrup balance and the cyclonic gyre in the Sea of Okhotsk. *J. Phys. Oceanogr.*, **34**, 513–525.

Ohshima, K. I., Y. Fukamachi, T. Mutoh and M. Wakatsuchi (2005): A generation mechanism for mesoscale eddies in the Kuril Basin of the Okhotsk Sea: Baroclinic instability caused by enhanced tidal mixing. *J. Oceanogr.*, **61**, 247–260.

Parkinson, C. L. and A. J. Gratz (1983): On the seasonal sea ice cover of the Sea of Okhotsk. *J. Geophys. Res.*, **88**, 2793–2802.

Schlax, M. G. and D. B. Chelton (1994): Aliased tidal errors in TOPEX/POSEIDON sea surface height data. *J. Geophys. Res.*, **99**, 24,761–24,776.

Simizu, D. and K. I. Ohshima (2002): Barotropic response of the Sea of Okhotsk to wind forcing. *J. Oceanogr.*, **58**, 851–860.

Simizu, D. and K. I. Ohshima (2006): A model simulation on the circulation in the Sea of Okhotsk and the East Sakhalin Current. *J. Geophys. Res.*, doi:10.1029/2005JC002980 (in press).

Smith, S. D. (1988): Coefficients for sea surface wind stress, heat flux and wind profiles as a function of wind speed and temperature. *J. Geophys. Res.*, **93**, 15,467–15,472.

Talley, L. D. (1991): Okhotsk Sea water anomaly: Implications for ventilation in the North Pacific. *Deep-Sea Res.*, **38**, Suppl. 1, 171–190.

Talley, L. D. and Y. Nagata (1995): The Okhotsk Sea and Oyashio Region. *PICES Sci. Rep.*, PICES, Sydney, B.C., Canada, 2, 227 pp.

Uchida, H. and S. Imawaki (2003): Eulerian mean surface velocity field derived by combining drifter and satellite altimeter data. *Geophys. Res. Lett.*, **30**, 1229, doi:10.1029/2002GL016445.

Uchimoto, K., H. Mitsudera, N. Ebuchi and Y. Miyazawa (2006): Clockwise eddy caused by the Soya Warm Current in an OGCM. *J. Oceanogr*. (submitted).

Wakatsuchi, M. and S. Martin (1990): Satellite observations of the ice cover of the Kuril Basin region of the Okhotsk Sea and its relation to the regional oceanography. *J. Geophys. Res.*, **95**, 13,393–13,410.

Wakatsuchi, M. and S. Martin (1991): Water circulation of the Kuril Basin of the Okhotsk Sea and its relation to eddy formation. *J. Oceanogr. Soc. Japan*, **47**, 152–168.

Watanabe, K. (1963): On the reinforcement of the East Sakhalin Current preceding to the sea ice season off the coast of Hokkaido—Study on the sea ice in the Okhotsk Sea (IV). *Ocenogr. Mag.*, **14**, 117–130.